Identification of metabotropic glutamate receptors at ribbon synapses of inner hair cells

Lisa Klotz [1], Olaf Wendler [2], Renato Frischknecht [3], Ryuichi Shigemoto [4], Francesco Ferraguti [5], Holger Schulze [6] and Ralf Enz [1]*

[1]Institute for Biochemistry (Emil-Fischer-Zentrum), Friedrich-Alexander University Erlangen-Nürnberg, Erlangen, Germany

[2]Department of Otorhinolaryngology, Head and Neck Surgery, Div. of Phoniatrics and Pediatric Audiology, Friedrich-Alexander University Erlangen-Nürnberg, Erlangen, Germany

[3]Department of Biology, Animal Physiology Friedrich-Alexander University Erlangen-Nürnberg, Erlangen, Germany

[4]Institute of Science and Technology (IST Austria), Klosterneuburg, Austria

[5]Department of Pharmacology, Medical University of Innsbruck, Innsbruck, Austria

[6]Department of Otorhinolaryngology, Head and Neck Surgery, Experimental Otolaryngology, Friedrich-Alexander University Erlangen-Nürnberg, Erlangen, Germany

***Corresponding author:** Ralf Enz
Institut für Biochemie
FAU Erlangen-Nürnberg
Fahrstrasse 17, 91054 Erlangen, Germany
Phone: +49-9131/85-24185
Fax: +49-9131/85-22485
E-Mail: ralf.enz@fau.de

Running Title: mGluR types at inner hair cell synapses

Keywords: cochlea, inner hair cell, metabotropic glutamate receptor, mGluR, ribbon synapse

Count: 27.172 + 7.663 characters

Abbreviations: aa - amino acids; CtBP2 - C-terminal binding protein 2, GABA - gamma-aminobutyric acid, IHC - inner hair cells, mGluR: metabotropic glutamate receptor; OHC - inner hair cells, PBS - phosphate-buffered saline; PFA - paraformaldehyde; PSD95 - post-synaptic density protein 95, STED - stimulated emission depletion

ABSTRACT

Glutamate is the major excitatory neurotransmitter in the central nervous system binding to a variety of glutamate receptors. Metabotropic glutamate receptors (mGluR1 to mGluR8) can act excitatory or inhibitory, depending on associated signal cascades. Expression and localization of inhibitory acting mGluRs at inner hair cells (IHC) in the cochlea is largely unknown. Here, we analysed expression of mGluR2, mGluR3, mGluR4, mGluR6, mGluR7 and mGluR8 and investigated their localization in respect to the pre-synaptic ribbon of IHC synapses. We detected transcripts for mGluR2, mGluR3, mGluR4, and for mGluR7a, mGluR7b, mGluR8a and mGluR8b splice-variants. Using receptor specific antibodies in cochlear wholemounts, we found expression of mGluR2, mGluR4 and mGluR8b close to pre-synaptic ribbons. Super resolution and confocal microscopy in combination with 3D reconstructions indicated a post-synaptic localization of mGluR2 that overlaps with PSD95 on dendrites of afferent type I spiral ganglion neurons. In contrast, mGluR4 and mGluR8b were expressed at the pre-synapse close to IHC ribbons. In summary, we localized in detail three mGluR types at IHC ribbon synapses, providing a fundament for new therapeutical strategies that could protect the cochlea against noxious stimuli and excitotoxicity.

INTRODUCTION

Within the mammalian cochlea the mechanosensory hair cells are typically organized into a single row of inner hair cells (IHC) and three rows of outer hair cells (OHC). While IHC are connected predominantly by afferences of bipolar type I spiral ganglion neurons that transmit the acoustic information to the brain stem, OHC mostly contact efferent neurons and are believed to function as cochlear amplifiers [1]. Upon stimulation, ribbon synapses of hair cells release the excitatory neurotransmitter glutamate that binds to ionotropic (ion channel associated) and metabotropic (G-protein coupled) glutamate receptors.

Ionotropic glutamate receptors preferentially mediate fast excitatory synaptic transmission, while metabotropic glutamate receptors (mGluRs) modulate neuronal excitability, synaptic plasticity and transmitter release [2]. The eight known mGluR types are subdivided into three groups: Group I - mGluR1 and mGluR5, group II - mGluR2 and mGluR3, group III - mGluR4, mGluR6, mGluR7 and mGluR8 [3]. While group I receptors positively modulate the activity at glutamatergic synapses, members of group II and group III preferentially reduce neurotransmitter release. These diverse functions can be derived from their specific expression at glutamatergic synapses: Generally, group I receptors are expressed at the post-synapse, members of group II were found both pre- and post-synaptically and group III mGluR types show a clear preference for the pre-synaptic terminal [4]. An exception is mGluR6: Within the central nervous system this receptor is expressed exclusively in the retina at post-synaptic sites of ON bipolar cells [5].

While the cochlear distribution and function of ionotropic glutamate receptors is well described (see e.g. [6,7]), most studies analysing their metabotropic counterparts focussed on the group I receptors mGluR1 and mGluR5 (see e.g. [8]). Much less is known about receptors belonging to group II (mGluR2 and mGluR3) and group III (mGluR4, mGluR7 and mGluR8) types in the cochlea: One study suggested the presence of group II mGluRs in efferent lateral olivocochlear GABAergic fibres that in turn inhibit dopaminergic efferences signalling onto IHC afferences [9]. Polymorphisms in mGluR7 were correlated with age-related hearing deficits or noise-induced hearing loss in humans [10-13]. Furthermore, a general expression of mGluR7 and mGluR8 in inner and outer hair cells was observed, but a synaptic localization of the receptors was not investigated [12,14]. Obviously, a comprehensive study regarding expression and synaptic localization of group II/III receptors in the cochlea is missing.

Therefore, here we analysed the expression of the group II and group III mGluR types in the mouse cochlea. In addition, we investigated in detail the distribution of corresponding receptor proteins with respect to the pre-synaptic ribbon of IHC in cochlear wholemounts of adult gerbils and mice. Group II and group III mGluR types are predestinated to protect against excitotoxic effects caused by over-stimulation and excessive glutamate release from

IHC, which could cause neurodegeneration and hearing impairment [15,16]. Thus, our detailed description of group II and III mGluRs at IHC ribbon synapses offers new therapeutical appraoches for the treatment of hearing impairments.

RESULTS

Group II and group III metabotropic glutamate receptors are expressed in the mouse cochlea

Several studies describe functions of group I mGluRs (mGluR1 and mGluR5) in the cochlea (see e.g. [8]). However, there are no comprehensive studies regarding expression of group II and III receptors in this tissue. Therefore, here we analysed in detail expression and localization of group II (mGluR2, mGluR3) and group III (mGluR4, mGluR6, mGluR7, mGluR8) receptors in the cochlea of mouse and gerbil.

To pave the ground for successive anatomical studies, we first tested the presence of group II and III mGluR types in the mouse cochlea, including common splice variants. Fig. 1 shows specific PCR amplificates for mGluR2, mGluR3, mGluR4 and for the receptor isoforms mGluR7a, mGluR7b and mGluR8a and mGluR8b. MGluR6 was not detectable in the cochlea, in line with its specific expression in bipolar cells of the retina within the central nervous system [5].

Next, we analysed the distribution of cochlear group II and III mGluRs with respect to the ribbon synapse of IHC. Our studies were guided by the quality and specificity of available immune sera. We used antibodies recognizing a conserved epitope in mGluR2 and mGluR3, in the following designated mGluR2/3, antibodies specific for mGluR2, mGluR3, mGluR4 and immune sera detecting mGluR8a or mGluR8b isoforms. Antibodies for mGluR2/3, mGluR4, mGluR8a and mGluR8b were well characterized and used before by several groups, including ourselves and thus are supposed to be specific [17-19]. Nevertheless, we again tested the quality of the immunsera using primary cultures of cortical neurons and antibodies binding Shank 2 to label post-synaptic sites (Fig. S1). The immune serum used in the past to detect mGluR7 in neuronal tissue, e.g. the retina [20] is not available anymore. Since currently available immune sera cannot reproduce the original data, mGluR7 was omitted from our studies.

Group II mGluR types show a synaptic expression in cochlear wholemounts

The antibodies recognizing a conserved epitope in the group II receptors mGluR2 and mGluR3 (mGluR2/3) bind to a linear stretch of amino acids conserved in their C-termini, preventing a distinction between these two mGluR types. While mGluR2 or mGluR3 specific antibodies are available, these sera are less characterized. Therefore, we performed all initial studies involving 3D reconstructions with the reliable mGluR2/3 serum, while the identity of the group II mGluR type was determined in separate stainings using antibodies specific for mGluR2 or mGluR3.

Gerbils are a well studied animal model in hearing resaerch. Thus, we marked pre-synaptic sites of IHC in cochlear wholemounts of the gerbil by antibodies specific for CtBP2/RIBEYE, the main protein of synaptic ribbons [21]. Co-labelling the same tissue for mGluR2/3 resulted in a punctate label that was always observed in close vicinity to the CtBP2 positive pre-synaptic ribbon of IHC (Figs. 2A, 2B). Given the prominent signal intensity for mGluR2/3, we next analysed the distribution of the receptors in the much smaller mouse cochlea (Figs. 2C, 2D). Comparing the spatial distribution of the relative signal intensities obtained for mGluR2/3 and CtBP2 showed a partial overlap of both signals (Figs. 2 b', b'', d', d''). This observation would be consistent with 2 possible localizations of mGluR2/3 relative to the synaptic cleft: (i) a pre-synaptic expression outside the active zone towards the annulus of the pre-synaptic terminal, or (ii) a post-synaptic expression of mGluR2/3 opposite to the pre-synaptic ribbon.

Signals for mGluR2/3 are present at post-synaptic sites of inner hair cell ribbon synapses

Since the mGluR2/3 staining patterns were comparable between the gerbil and mouse, in the following we used mouse tissue only. To distinguish between a pre- versus post-synaptic expression of mGluR2/3 at IHC synapses, we analysed the receptors´ distribution in more detail using stimulated emission depletion (STED) microscopy. Cochlear wholemounts from mouse were co-stained with antibodies recognizing mGluR2/3 and the CtBP2/RIBEYE immune serum used above, which marks the pre-synaptic ribbon (Fig. 3A-E). To stain post-synaptic specializations formed by afferent type I spiral ganglion neurons that are located opposite to the pre-synaptic ribbon we used antibodies recognizing the post-synaptic density protein PSD95 [22] (Fig. 3A and 3F-H). Z-stacks obtained from dual-colour STED microscopy were 3D reconstructed and distances from the centres of gravity were measured, as exemplified by the dots shown in Fig. 3C and 3F. While the mean distance between mGluR2/3 and pre-synaptic ribbons was between 138 to 428 nm (mean of 258 ± 88.6 nm), the distance between the receptors and PSD95 was significantly smaller (81.8 ± 31.0 nm; Fig. 3I). These data favour a post-synaptic expression of mGluR2/3, slightly displaced from the PSD95 labelled active zone.

In order to strengthen this assumption, we labelled simultaneously pre- and post-synaptic terminals using the marker antibodies shown in Fig. 4A and compared resulting fluorescent signals with the expression of mGluR2/3. Unfortunately, the available STED microscope allowed the simultaneous detection of 2 colour channels only. Therefore, we switched back to classical confocal microscopy in combination with 3D reconstruction. Cochlear wholemounts of mice were incubated with antibodies binding to mGluR2/3, CtBP2/RIBEYE

and PSD95 and the geometry of individually labelled synapses was 3D reconstructed from the confocal images (Fig. 4A, B). Reconstructions of the CtBP2/RIBEYE label showed that the size of the pre-synaptic ribbons was elongated into one direction, a feature that was observed by other groups before [23]. This is represented in Figs. 4C and 4D that compare the same synapse horizontally rotated by about 90 degrees. Examples of more ribbon synapses are summarized in Fig. 4E. In all synapses analysed, we observed a clear overlap of mGluR2/3 with the post-synaptic marker PSD95, which was clearly separated from the pre-synaptic CtBP2/RIBEYE labelled ribbon.

Interestingly, mGluR2/3 was not completely co-localized with PSD95, but always shifted laterally. PSD95 marks the active zone within synapses that contains e.g. AMPA type glutamate receptors, while mGluR2/3 seem to be expressed just adjacent to the release site of glutamate. To quantify these observations, we calculated the centres of gravity for reconstructed signals of CtBP2/RIBEYE, PSD95 and mGluR2/3 at more than 40 individual ribbon synapses, represented by white dots as shown in Fig. 4D. The mean distance between the pre- and post-synaptic markers CtBP2/RIBEYE and PSD95 (274 ± 89.0 nm) was comparable to the distance between CtBP2 and mGluR2/3 (279 ± 86.1 nm; Fig. 4F). In contrast, the mean distance between PSD95 and mGluR2/3 was significantly shorter (164 ± 32.2 nm), indicating that these 2 proteins are localized at the same side of the synaptic cleft. Calculating the angels between the 3 centres of gravity showed similar values for beta (74.0 ± 19.8 degrees) and gamma (71.4 ± 22.8 degrees; Figs. 4F) that were significantly different from alpha (34.6 ± 10.8 degrees), being consistent with a post-synaptic localization of mGluR2/3.

Next, we exchanged CtBP2/RIBEYE with Bassoon as another pre-synaptic marker that is involved in anchoring the ribbon to the pre-synaptic membrane (Fig. 4A) [23,24]. Label for mGluR2/3 did overlap with PSD95, but not with Bassoon (Fig. 4G). Measuring distances and angles between the centres of gravity of signals obtained from several synapses suggested that mGluR2/3 are present in close vicinity to PSD95 (mean of 140 ± 24.8 nm), while being significantly more distant to Bassoon (mean of 272 ± 104 nm) (Fig. 4H). As before, the closest angle was alpha (34.3 ± 15.9 degrees), being significantly smaller that beta (66.9 ± 21.2 degrees), or gamma (78.8 ± 17.1 degrees). Our data are consistent with mGluR2/3 being localized at the same side of the synaptic cleft as PSD95. We conclude that mGluR2/3 is expressed at the post-synaptic side of IHC ribbon synapses, directly adjacent to the active zone.

Expression of mGluR2/3 does not change along the tonotopic axis

It has been shown that the number of ribbon synapses per IHC varies along the tonotopic axis in the cochlea of mouse and gerbil [25]. Therefore, we asked if the expression of mGluR2/3 at these synapses might also change along the spectral gradient. To this end, we co-stained cochlear wholemounts of mice for CtBP2/RIBEYE and mGluR2/3, as above. Three different tonotopic locations of the cochlea (apex, medial and base) were selected and the number of fluorescent puncta representing CtBP2/RIBEYE or mGluR2/3 were counted, as indicated in Fig. 5A to C. Finally, the number mGluR2/3 positive puncta obtained from the individual micrographs was normalized to the number of detected IHC ribbons. Fig. 5D shows that (i) we detected mGluR2/3 specific signals at 94% to 98% of IHC ribbon synapses and (ii) that these numbers did not change significantly along the tonotopic axis.

MGluR2/3 specific signals are not present at efferent terminals contacting IHC synapses

Previously, mGluR2/3 were proposed to be expressed by GABAergic neurons that inhibit dopaminergic efferences [9]. Although expression of these receptors was not detected directly, the authors suggested that group II mGluRs could be activated by a spill-over of glutamate released from the nearby IHC ribbon synapse. This, in turn would reduce the release of GABA, leading to a disinhibition in dopaminergic terminals. Thus, we tested if the lateral shift observed in the localization of mGluR2/3 in respect to PSD95 (see Figs. 3F to I and 4C to H) could be explained by the expression of the receptors in efferent terminals contacting the IHC ribbon synapse, rather than being present at the afferent IHC post-synapse. To this end, we marked olivocochlear efferent terminals with antibodies recognizing Synapsin 1 [26]. Co-staining cochlear wholemounts from mice for mGluR2/3, Synapsin 1, CtBP2/RIBEYE and PSD95 in different combinations did not show any obvious co-localization of the receptors with Synapsin 1 labelled efferent terminals (Fig. 6A - D). While we cannot rule out a low expression level at olivocochlear efferent terminals, we conclude that the majority of mGluR2/3 is present at the IHC post-synapse.

MGluR2, but not mGluR3 can be detected at IHC ribbon synapses

The mGluR2/3 immune serum used in this study was generated against a C-terminal sequence from mGluR2 that is highly conserved in mGluR3. Since we detected transcripts for both group II receptors in the cochlea (see Fig. 1), we next investigated if both receptors would be actually present at IHC synapses, using receptor specific antibodies. Because the mGluR2 and mGluR3 specific immune sera are not used to the same extend in the scientific

literature as the well-established mGluR2/3 serum, we ensured that the antibodies would be receptor specific and able to bind to the native receptor epitope in neurons, using HEK-293 cells and cortical neurons in culture (Figs. S1 and S2).

Co-staining of cochlear wholemounts for CtBP2/RIBEYE, mGluR2 or mGluR3 showed that only signals derived from the mGluR2/3 and mGluR2 sera were detectable in close vicinity to IHC ribbons (Fig. 7A-D). In contrast, mGluR3 fluorescence appeared more diffuse and was not co-localized with synaptic ribbons (Fig. 7E). Given the lower intensity of mGluR3 specific signals in the cochlea, we tested this serum on cortical neurons, as mentioned in the previous paragraph. Co-labelling synapses for the post-synaptic marker protein Shank 2 showed a co-localization with the binding sites of the mGluR3 antibodies (Fig. 7F), indicating that the serum is able to recognize the native receptor epitope in a neuronal context. This observation is in agreement with previous studies that described mGluR3 in primary cultures of cortical neurons [27,28]. These data suggest that mGluR2, but not mGluR3 is present at the post-synaptic side of IHC ribbon synapses.

MGluR4 and mGluR8b are expressed at the pre-synaptic side of IHC ribbon synapses

Finally, we analysed the localization of mGluR4, mGluR8a and mGluR8b in the cochlea. Immune sera for mGluR4 and mGluR8b were demonstrated before to specifically recognise their target proteins (Corti *et al.* 2002, Ferraguti *et al.* 2005). Here, we tested if the mGluR8a serum would be reliable, as well. Using HEK-293 cells and cortical neurons in culture, we showed that the mGluR8a antibodies do not bind to mGluR8b and that they recognize the native receptor epitope in neurons (Figs. S1 and S3).

These immune sera were then applied to cochlear wholemounts and pre-and post-synaptic specializations were marked for CtBP2/RIBEYE and PSD95, as before. Fluorescent signals representing the different mGluR types appeared as puncta, indicating a synaptic localization of these receptors (Figs. 8A, 9A and 9B). However, only mGluR4 and mGluR8b, but not mGluR8a were in close vicinity to CtBP2/RIBEYE and PSD95. Interestingly, in contrast to the partial overlap of mGluR2/3 with the pre-synaptic ribbon at IHC ribbon synapses shown in Fig. 4, signals representing mGluR4 or mGluR8b are completely superimposed with the pre-synaptic ribbon marker CtBP2/RIBEYE (Fig. 8B, 9C), while overlapping only partially with the post-synaptic PSD95 (Fig. 8C, 9D). This suggested a pre-synaptic localization of the two receptors at IHC ribbon synapses.

Indeed, after reconstructing the geometry of the labelled proteins at individual synapses, we observed a clear overlap of mGluR4 and mGluR8b with the pre-synaptic CtBP2/RIBEYE labelled ribbon, while the receptors were more distant to the post-synaptic marker PSD95 (Figs. 8D, E and 9E, F). As before, the centres of gravity of the reconstructed fluorescent

labels representing the receptors, CtBP2/RIBEYE or PSD95 were calculated for individual ribbon synapses and distances and angles between these centres were measured, as indicated in Figs. 8D and 9E. The mean distance between mGluR4 or mGluR8b and the pre-synaptic marker CtBP2/RIBEYE was significantly shorter (mGluR4: 108 ± 23.4 nm; mGluR8b: 119 ± 54.5 nm) than the distance between the receptors and the post-synaptic label (mGluR4: 373 ± 123 nm; mGluR8b: 317 ± 53.9 nm; Figs. 8F and 9G). Comparing the angels between the 3 centres of gravity revealed the smallest number at the gravity centre for PSD95 (mGluR4: 14.7 ± 9.1 degrees; mGluR8b: 20.5 ± 10.8 degrees; Figs. 8G and 9H). These data are consistent with a pre-synaptic localization of mGluR4 and mGluR8b.

DISCUSSION

In sensory organs like retina and cochlea, the intensity of a given stimulus is encoded by the graded amount of the neurotransmitter glutamate released at ribbon synapses of photoreceptors or inner hair cells (IHC), respectively. While expression and function of the inhibitory group II and III mGluR types at the photoreceptor ribbon synapse is well described (see e.g. [29,30]), much less information is available for the ribbon synapse of IHC. Here we analysed the expression and localization of group II and III mGluRs in cochlear wholemounts in respect to the pre-synaptic ribbon of IHC.

We identified transcripts encoding mGluR2, mGluR3, mGluR4, as well as common mGluR7 and mGluR8 isoforms in the mouse cochlea. Furthermore, we localized mGluR2, mGluR4 and mGluR8b proteins at pre- or post-synaptic sides of the IHC ribbon synapse. A distinction between pre- and post-synaptic receptor expression was facilitated by the fact that the used antibodies recognize an epitope in the intracellular C-termini of mGluR2, mGluR4 and mGluR8b. Thus, corresponding labels appear at the intracellular sides of pre- or post-synaptic membranes, resulting in the maximal possible distance between the two compartments. Indeed, we could clearly separate pre- and post-synaptic marker proteins by our microscopy techniques.

MGluR2 was present at post-synaptic afferent processes of type I spiral ganglion neurons that contact the IHC ribbon synapse. There, mGluR2 specific signals partially overlapped with the post-synaptic marker protein PSD95. While PSD95 was located opposite to the pre-synaptic ribbon, as described before [31], mGluR2 specific labelling was shifted laterally. This is in agreement with the idea that group II mGluRs are generally located outside the active zone of glutamatergic synapses [32]. A pre-synaptic expression of group II mGluRs is widely accepted [33]. A recent study analysing group II receptors in layer III of the primate dorsolateral prefrontal cortex found mGluR2 mostly at the pre-synapse of glutamatergic neurons, while mGluR3 was expressed preferentially at the post-synaptic specializations of spines [34]. The authors conclude that mGluR2 functions predominantly as autoreceptor, reducing neuronal excitation and glutamate release upon activation. However, in other CNS regions, mGluR2 was observed at post-synaptic sites [4,35-37]. Our study ads ribbon synapses of IHC as another location within the CNS that shows a post-synaptic expression of mGluR2.

Besides cochlear hair cells, also photoreceptors and bipolar cells of the retina form ribbon synapses [38]. In both tissues, mGluR2 was observed at the post-synaptic side of ribbon synapses, while mGluR3 was absent from this synapse type (this study and [37,39]). Unlike the cochlea however, in the retina mGluR2 is not present at the ribbon synapse of sensory cells (photoreceptors), but expressed at ribbon synapses formed by second order neurons, designated as bipolar cells [37].

In contrast to mGluR2, we detected mGluR4 at the pre-synaptic side of IHC ribbon synapses. Again, the situation is different in the retina. Ribbon synapses of photoreceptors in the mammalian retina do not express mGluR4. Instead, this receptor is present at the post-synaptic side of ribbon synapses formed by bipolar cells, similar to mGluR2, as described in the previous paragraph [37,40].

Ribbon synapses of photoreceptors express mGluR8 at their pre-synaptic site [29]. There, the receptor functions as integral part of a negative feed-back loop, reducing intracellular calcium concentrations via a pertussis toxin sensitive G-protein, thereby regulating the glutamate concentration in the synaptic cleft [41]. The immune serum used was directed against 19 amino acids in the C-terminus of the mGluR8a isoform (residues 890–908: ETNTSSTKTTYISYSDHSI) [29]. While the N-terminal 3 amino acids are identical between mGluR8a and mGluR8b, the remaining sequence is specific for the mGluR8a isoform. Thus, we assume that in this study actually the distribution of mGluR8a, not mGluR8b was described. We are not aware of any previous study describing in detail the localization of mGluR8b at ribbon synapses in the CNS, or of mGluR8b associated signal cascades. Recently, we identified cytosolic proteins that bind to mGluR8 types in an isoform specific way: CRIP1a regulated the endocytosis behaviour of mGluR8a, but not of mGluR8b [42]. While CRIP1a was detected at the photoreceptor pre-synapse [43], its expression in the cochlea has not been investigated. In contrast to CRIP1a, the SUMO E3-ligases PIAS1 and PIAS3L interacted only with the mGluR8b isoform, but not with mGluR8a [44]. Thus, we speculate that IHC in the cochlea and photoreceptors in the retina express different mGluR8 isoforms at their ribbon synapses that permit a distinct regulation of associated signal cascades.

In recent years it became increasingly clear that mGluRs exist as constitutive dimers [45]. Dimerization of mGluRs seems to be a pre-requisite for receptor activation and function [46]. Besides the formation of homodimers, the authors observed the assembly of different mGluR types into heterodimeric receptor complexes: Members of group I (mGluR1 and mGluR5) can form homo- and heterodimers with themselves, but not with group II or III receptors. Vice versa, most of the group II and III receptors can form homo- and heterodimers with partners of these 2 groups, but not with group I receptors. While the above mentioned receptor dimers were observed using heterologous expressed receptors in cell lines [47], the existence of mGluR2/mGluR4 heterodimers was shown in neurons [48]. We observed mGluR2 and mGluR4 at opposite sides of the synaptic cleft, excluding a heterodimerization between these two receptors at the IHC ribbon synapse. On the other hand, mGluR4 and mGluR8b are both expressed pre-synaptically, in principle enabling the formation of heterodimers. Unfortunately, the nature of available immune sera prevented direct co-localization of mGluR4 and mGluR8b.

Certain mGluRs heterodimerize with other GPCR types, including serotonin, dopamine and adenosine receptors [49]. MGluR2 forms heterodimers with the 5-HT2A serotonin receptor using 3 amino acids present within the receptors transmembrane domain 4 [50,51]. However, 5-HT2A receptors are not expressed in the mouse cochlea [52]. While serotonin and serotonin synthetizing enzymes, such as tryptophan hydroxylase were detected in afferent spinal ganglion neurons (see e.g. [53]), we found no evidence in the literature that these neurons express serotonin receptors at ribbon synapses of IHC in the cochlea. In contrast to the cochlea, ribbon synapses of photoreceptors and bipolar cells in the rabbit retina do express 5-HT2A receptors [54].

For proper function, mGluRs interact with a variety of intracellular binding partners that regulate receptor trafficking, their synaptic localization, agonist sensitivity and desensitization behavior, as well as the efficacy of G-protein coupling [55]. Several proteins binding to the intracellular C-termini of mGluR2, mGluR4 and mGluR8b were identified by us and others, including the aforementioned CRIP1a and E3-ligases of the SUMOylation cascade, as well as GRIP, PICK1, Syntenin and cytoskeleton associated proteins such as MAP1B and band 4.1 proteins [42,44,56,57]. Of these, band 4.1 proteins were detected in IHC of the mouse cochlea and associated with hearing deficits [58,59]. The authors localized band 4.1B, 4.1G, 4.1N and 4.1R at stereocilia and point out the 4.1R interacts with myosin XV and with whirlin, two proteins associated with deafness. Previously, we described band 4.1 proteins as new binding partners of mGluR8 isoforms [57]. Upon binding, 4.1B increased the surface expression of mGluR8b and inhibited the receptors´ G-protein signaling. Although the presence of band 4.1 proteins at IHC ribbon synapses has not been analyzed so far, the above cited studies show that all four band 4.1 proteins are expressed in IHC, in principle enabling an interaction with and a regulation of mGluR8b.

Our 3D reconstructions of CtBP2 fluorescent signals showed that the pre-synaptic ribbon is elongated into one direction, which has been described previously [23,25]. Based on electron microscopic data from IHC ribbons located in the midchochlear region, Meyer and co-workers calculated mean values for the long (228 ± 60 nm) and short (118 ± 27 nm) axis of the pre-synaptic ribbon. In addition, the post-synaptic density opposite to the pre-synaptic ribbon of IHC was measured to be about 610nm in length [23]. Although a detailed evaluation of the dimensions of the pre- and post-synaptic structures was not of principle interest of this study, the geometry of our 3D reconstructions for CtBP2 and PSD95 are in agreement the studies cited above.

A recent study describes functional roles of Gαi proteins at IHC ribbon synapses, influenceing synaptic ribbons, synapse size and neuronal excitability [60]. The authors showed that disruption of Gαi3 signalling increased the number of calcium channel clusters

and the size of the active zone. Since mGluR2, mGluR4 and mGluR8b can signal via Gαi proteins, these receptors might guide the activity of Gαi3 in IHC.

Defects in hearing or vision were not reported in mice lacking mGluR2, mGluR3, mGluR4 and mGluR8 (see e.g. [40,61-64]). This indicates that these receptors are not primarily involved in transmitting sensory information to higher brain areas, but might be more relevant in modulating more general aspects in sensory neurons, e.g. synaptic sensitivity. In doing so, the receptors could protect IHC ribbon synapses against over-stimulation and resulting excitotoxic effects. Besides a genetic predisposition and inflammation, also mechanical insult such as noise trauma can disturb and lead to a dysfunction of the cochlear neurotransmitter systems [65,66]. Intense acoustic stimuli cause a strong pre-synaptic glutamate release at the IHC ribbon synapse, which could over-stimulate post-synaptic ionotropic glutamate receptors [23,25]. This in turn would result in an unphysiologically high influx of calcium ions into post-synaptic terminals, leading to an over-excitation of spiral ganglion neurons. Furthermore, unphysiologically high calcium concentrations can activate intracellular signal pathways that induce apoptotic cell death, ultimately leading to acute hearing loss [65,67,68]. Fortunately, besides efferent innervations formed by inhibitory olivocochlear reflex loops [69], the cochlea contains inhibitory feedback loops organized locally at synapses that regulate activity and survival of sensory neurons and protect against noxious stimuli and excitotoxicity [70]. The detected mGluR2, mGluR4 and mGluR8b at the IHC ribbon synapse are well suited for this task, since these receptors can invert the activity of the excitatory neurotransmitter glutamate into neuronal inhibition, using intracellular signal cascades.

MATERIALS AND METHODS

Experiments were carried out in accordance with the guidelines of the University Erlangen-Nürnberg and the Deutsche Forschungsgemeinschaft.

Molecular biology

For RNA isolation, cochleae were dissected from the temporal bone and immediately frozen in liquid nitrogen. Total RNA from 3 cochleae of mice was homogenized using Minilys Personal Homogenizer (Bertin Instruments, Montigny-le-Bretonneux, France) and extracted with the RNeasy Micro Kit (Qiagen, Hilden, Germany). Genomic DNA was removed by digestion with DNAse and cDNA synthesis was performed using the QuantiTect Reverse Transcription Kit (Qiagen) and random hexameres/oligo-dT. PCR amplification was performed with 3 µl (40 ng) reverse transcribed RNA in 50 µl of PCR-buffer (in mM: 20 Tris-HCl, 50 KCl, 2 $MgCl_2$, 0.2 dNTPs), 0.2pM each primer (see Tab. 1), 10 Units Taq-polymerase (Invitrogen, Waltham, MA), pH = 8.0) in a thermocycler (Applied Biosystems, Foster City, CA) using the following parameters: 94°C for 2 min followed by 35 cycles at 94°C for 45 s, 60°C for 60 s, 72°C for 60 s and a final incubation at 72°C for 10 min. Five microliters of each PCR-product were separated on a 1.5% agarose gel. Primer pairs amplify a C-terminal region of the receptor sequences and were designed to span introns to detect residual chromosomal DNA contaminations (Tab. 1). Primer pairs for mGluR2, 3, 4, 7a, 7b, 8a and 8b were successfully tested with mouse brain cDNA, or with a plasmid sequence for the retina specific mGluR6 (not shown). Control amplifications (H_2O) showed no specific PCR products. All PCR amplificates were identified by DNA sequencing.

Immunocytochemistry

For immunofluorescence staining, animals were sacrificed and the cochleae were dissected using a stereomicroscope. Thereafter, 4 % paraformaldehyde (PFA) in phosphate-buffered saline (PBS) was applied over the round window. Cochleae of adult gerbils were fixed for 1h and of adult mice (6 - 12 weeks) for 15 min on ice. Thereafter, the cochlea was opened near the apex, explanted and decalcified in 140 mM EDTA at 4°C overnight. Gerbil cochlea turns were cut into three pieces after decalcification. Samples were blocked for 1 h in 5 % horse serum and 0.3 % Triton X-100 in PBS. Primary antibodies were diluted in in 0.1 % horse serum, 0.1 % Triton X-100 in PBS and applied overnight at 4°C, as specified in Table 2. Secondary antibodies (Alexa Fluor-488 conjugated anti-mouse or rabbit, Cy3 or Alexa Fluor-568 conjugated anti-mouse or guinea-pig, Alexa-Fluor-647 conjugated anti-goat or mouse were diluted as above with DAPI and applied for 1 h at room temperature (secondary antibodies were purchased from molecular probes, Invitrogen, Dianova, or Jackson

Immunoresearch). Finally, samples were mounted with Aqua Poly/Mount (Polysciences Inc., Warrington, PA).

Fluorescent labels were visualized with a Zeiss Axio Imager Z2 (Zeiss, Oberkochen, Germany) equipped with an ApoTome by using ZEN blue 2012 software. Images were taken with a 63× objective (1.4 oil, Apochromat, Zeiss) and z-projections were calculated with ZEN software (Zeiss). To study three-dimensional protein distributions, images were taken with a Laser Scanning Microscope 710 (Zeiss) by using ZEN black 2010 software with corresponding imaging modules, a stack interval of 0.9 µm and a pinhole of 1 airy unit. 3D images were reconstructed from z-stacks using Imaris 8 (Bitplane, Concord, MA).

For high resolution STED microscopy, anti-rabbit STAR-580 1:200 and anti-mouse STAR-635P 1:200 (Abberior Instruments, Göttingen, Germany) were used as secondary antibodies and probes were mounted with mowiol dabco (Sigma-Aldrich, St. Louis, MO). Thereafter, cochlea wholemounts were analysed with a STED microscope (2-Channel Super Resolution Microscope, Abberior Instruments) equipped with with a 100× oil immersion lens (NA: 1.44). Probes were excited at 561nm and 640nm and stimulated emission depletion was performed at 775nm with a pulsed laser. Image stacks were acquired with Imspector Software (Abberior Instruments) in 3D STED-mode with a xyz pixel size from 90 x 90 x 90 nm. Deconvolution was performed in Huygens Professional 18.04 **(**Scientific Volume Imaging B.V., Netherlands**)** and images were reconstructed from z-stacks using Imaris 8 (Bitplane).

All antibody incubations of mouse cochlear wholemounts were repeated between 3 and 6 times, except incubations shown in Fig. 3. As control, cochleae were incubated with secondary antibodies only, which resulted in the absence of detectable fluorescence. Recorded fluorescent signals were assembled in Adobe Photoshop (CS5; Adobe Systems Inc., San Jose, CA) and contrast enhanced and enlarged, if needed for better visualization.

Cell culture

The specificity of immune sera directed against mGluR2, mGluR3, mGluR8a and mGluR8b was verified with HEK-293 cells transfected with plasmids encoding the receptors. HEK-293 cells were grown in 6 well plates at 37°C and 5 % CO_2 on glass coverslips coated with poly(L-lysine)/3-aminopropyltriethoxysilane in minimum essential media that was supplemented with 10% fetal bovine serum, L-glutamine and penicillin/streptomycin (Life Technologies, Grand Island, NY) to approximately 50 % confluency. Cells were transfected with 2 µg plasmid DNA encoding for the rat sequences of mGluR2 or mGluR3 (kindly provided by J.-P. Pin, Institut de Genomique Fonctionnelle, Montpellier, France), mGluR8a or mGluR8b (kindly provided by F. Ferraguti, Innsbruck, Austria) for 18 h using lipofection (jetPEI, Polyplus transfection, NY, USA). Thereafter, cells were washed three times with PBS

and incubated for another 48 h as above to allow protein expression. Then, cells were washed, fixed in 4 % (v/v) PFA/PBS for 10min on ice, washed again and blocked with 10 % (v/v) fetal bovine serum containing 2 % (w/v) bovine serum albumine and 0.1 % Triton X-100 for 30 min. Subsequently, cells were incubated for 1.5h at room temperature with primary antibodies diluted in blocking solution, as indicated in Figs. S2 and S3 (see Tab. 2 for details of the used immune sera). After washing, secondary antibodies (Alexa Fluor-488, conjugated anti-mouse or rabbit, Cy3 conjugated anti-mouse or rabbit) together with DAPI were diluted as above and applied for 45 min hour at room temperature.

All immune sera recognizing the different mGluR types analysed in this study were also tested on neurons. Cultures of cortical neurons were prepared from E18 Sprague-Dawley rats in Hank's balanced salt solution as previously described [71]. In brief, the cortex (excluding olfactory bulb and hippocampus) was dissected, washed in Hank's balanced salt solution (-Ca^{2+}, -Mg^{2+}) and incubated in Hank's balanced salt solution containing trypsin for 5 min (37°C). After trypsin removal cells were carefully dispersed in Dulbecco's modified Eagle's medium containing 10 % FCS. Cells were plated at a density of 100 x 10^3 cells per mL on poly(L-lysine) coated cover slips in a 24-well plate. Cultures were maintained in serum-free neurobasal medium (Invitrogen) containing GS21 supplement (Sigma) and kept at 37°C in 5 % CO_2.

After 14-21 days in culture, cells were washed, fixed in 4 % PFA/PBS for 10min on ice and incubated with immune sera recognizing the mGluR types indicated in Fig. S1 and the post-synaptic marker protein Shank 2 (see Tab. 2 for antibody specifications) for 1.5 h at room temperature. The binding sites of the primary antibodies were visualized by secondary antibodies coupled to Alexa Fluor-488 conjugated rabbit, Alexa Fluor-568 conjugated anti-guinea-pig (Molecular Probes, Invitrogen). Coverslips containing stained cortical neurons were extensively washed and mounted with Aqua Poly/Mount (Polysciences Inc.). Fluorescent signals of stained HEK-293 cells and of cortical neurons were recored with a Zeiss Axio Imager Z2 (Zeiss) and assembled in in Adobe Photoshop (Adobe Systems Inc), as described above. As control, cells were incubated with a mixture of only secondary antibodies, which resulted in the absence of detectable signals.

Data analysis

The ImageJ tool "Plot Profile" was used to measure fluorescence profiles in individual confocal images (ImageJ version 1.49g; U. S. National Institutes of Health, Bethesda, Maryland, USA). 3D reconstructions of fluorescent signals of z-stacks from STED or confocal microscopy, the definition of the centres of gravity of reconstructed signals, as well as distance and angle measurements were performed with Imaris (Bitplane). Obtained data sets

were evaluated using the Microcal Origin Software (Microcal Software, Northhampton, MA). Statistical significance was calculated with the one-way ANOVA test. Errors are expressed as +/- SD.

ACKNOWLEDGEMENTS

We thank Jean-Philippe Pin für providing expression constructs encoding for mGluR2 or mGluR3 and the Optical Imaging Center Erlangen (OICE) for excellent scientific and technical support. This work was supported by the Deutsche Forschungsgemeinschaft (DFG) and the Interdisciplinary Centre for Clinical Research (IZKF) at the University Hospital of the Friedrich-Alexander-Universität Erlangen-Nürnberg. The authors declare no conflict of interest.

AUTHOR CONTRIBUTIONS

L.K. performed PCR experiments, prepared and stained cochlear wholemounts, transfected and stained HEK-293 cells, stained cortical neurons and performed microscopy analysis and 3D reconstructions, as well as data evaluation and interpretation. O.W. prepared cochlear wholemounts and assisted with antibody staining and microscopy. R.F. prepared cortical cultures. R.S. and F.F. generated and provided immune sera for mGluR4 and mGluR8b. H.S. designed experiments and interpreted the microscopy data. R.E. designed experiments, evaluated and interpreted the microscopy data, and wrote the paper. All authors read, revised and approved the manuscript.

CONFLICT OF INTEREST

The authors declare no conflict of interest.

REFERENCES

1. Fettiplace R (2017) *Comprehensive Physiology* **7:** 1197-1227
2. Reiner A, Levitz J (2018) *Neuron* **98:** 1080-1098
3. Enz R (2012) *Current drug targets* **13:** 145-156
4. Tamaru Y, Nomura S, Mizuno N*, et al.* (2001) *Neuroscience* **106:** 481-503
5. Martemyanov KA (2014) *Invest Ophthalmol Vis Sci* **55:** 8201-8207
6. Goutman JD, Elgoyhen AB, Gomez-Casati ME (2015) *FEBS Lett* **589:** 3354-3361
7. Takago H, Oshima-Takago T (2018) *Hearing research* **362:** 1-13
8. Lu Y (2014) *Neuroscience* **274:** 429-445
9. Doleviczenyi Z, Halmos G, Repassy G*, et al.* (2005) *Neuroscience letters* **385:** 93-98
10. Van Laer L, Huyghe JR, Hannula S*, et al.* (2010) *Eur J Hum Genet* **18:** 685-693
11. Yu P, Jiao J, Chen G*, et al.* (2018) *BMC medical genetics* **19:** 4
12. Friedman RA, Van Laer L, Huentelman MJ*, et al.* (2009) *Hum Mol Genet* **18:** 785-796
13. Newman DL, Fisher LM, Ohmen J*, et al.* (2012) *Hearing research* **294:** 125-132
14. Girotto G, Vuckovic D, Buniello A*, et al.* (2014) *PLoS One* **9:** e85352
15. Wan G, Corfas G (2015) *Hearing research* **329:** 1-10
16. Liberman MC, Kujawa SG (2017) *Hearing research* **349:** 138-147
17. Corti C, Aldegheri L, Somogyi P*, et al.* (2002) *Neuroscience* **110:** 403-420
18. Ferraguti F, Klausberger T, Cobden P*, et al.* (2005) *J Neurosci* **25:** 10520-10536
19. Seebahn A, Rose M, Enz R (2008) *FEBS Lett* **582:** 2453-2457
20. Brandstätter JH, Koulen P, Kuhn R*, et al.* (1996) *J Neurosci* **16:** 4749-4756
21. Schmitz F, Konigstorfer A, Sudhof TC (2000) *Neuron* **28:** 857-872
22. Martinez-Monedero R, Liu C, Weisz C*, et al.* (2016) *eNeuro* **3:**
23. Wong AB, Rutherford MA, Gabrielaitis M*, et al.* (2014) *EMBO J* **33:** 247-264
24. Khimich D, Nouvian R, Pujol R*, et al.* (2005) *Nature* **434:** 889-894
25. Meyer AC, Frank T, Khimich D*, et al.* (2009) *Nature neuroscience* **12:** 444-453
26. Vogl C, Cooper BH, Neef J*, et al.* (2015) *Journal of cell science* **128:** 638-644
27. Koga K, Iwahori Y, Ozaki S*, et al.* (2010) *J Neurosci Res* **88:** 2252-2262
28. Suzuki S, Koshimizu H, Adachi N*, et al.* (2017) *Peptides* **89:** 42-49
29. Koulen P, Kuhn R, Wässle H*, et al.* (1999) *Proc Natl Acad Sci U S A* **96:** 9909-9914
30. Brandstatter JH, Koulen P, Wassle H (1998) *Vision research* **38:** 1385-1397
31. Tong M, Brugeaud A, Edge AS (2013) *Journal of the Association for Research in Otolaryngology : JARO* **14:** 321-329
32. Ferraguti F, Shigemoto R (2006) *Cell Tissue Res* **326:** 483-504
33. Johnson KA, Lovinger DM (2016) *Frontiers in cellular neuroscience* **10:** 264
34. Jin LE, Wang M, Galvin VC*, et al.* (2018) *Cereb Cortex* **28:** 974-987
35. Petralia RS, Wang YX, Zhao HM*, et al.* (1996) *J Comp Neurol* **372:** 356-383
36. Petralia RS, Wang YX, Niedzielski AS*, et al.* (1996) *Neuroscience* **71:** 949-976
37. Koulen P, Malitschek B, Kuhn R*, et al.* (1996) *Eur J Neurosci* **8:** 2177-2187
38. tom Dieck S, Brandstatter JH (2006) *Cell Tissue Res* **326:** 339-346
39. Hartveit E, Brandstatter JH, Enz R*, et al.* (1995) *Eur J Neurosci* **7:** 1472-1483

40. Quraishi S, Gayet J, Morgans CW*, et al.* (2007) *J Comp Neurol* **501:** 931-943
41. Koulen P, Liu J, Nixon E*, et al.* (2005) *Investigative ophthalmology & visual science* **46:** 287-291
42. Mascia F, Klotz L, Lerch J*, et al.* (2017) *J Neurochem* **141:** 577-591
43. Hu SS, Arnold A, Hutchens JM*, et al.* (2010) *The Journal of comparative neurology* **518:** 3848-3866
44. Dütting E, Schröder-Kress N, Sticht H*, et al.* (2011) *The Biochemical journal* **435:** 365-371
45. Doumazane E, Scholler P, Zwier JM*, et al.* (2011) *Faseb J* **25:** 66-77
46. Moller TC, Moreno-Delgado D, Pin JP*, et al.* (2017) *Biophysics reports* **3:** 57-63
47. Yin S, Noetzel MJ, Johnson KA*, et al.* (2014) *J Neurosci* **34:** 79-94
48. Moreno Delgado D, Moller TC, Ster J*, et al.* (2017) *eLife* **6:**
49. Pin JP, Bettler B (2016) *Nature* **540:** 60-68
50. Gonzalez-Maeso J, Ang RL, Yuen T*, et al.* (2008) *Nature* **452:** 93-97
51. Moreno JL, Muguruza C, Umali A*, et al.* (2012) *J Biol Chem* **287:** 44301-44319
52. Oh CK, Drescher MJ, Hatfield JS*, et al.* (1999) *Brain Res Mol Brain Res* **70:** 135-140
53. Long L, Xie X, Tang Y (2018) *Indian journal of otolaryngology and head and neck surgery : official publication of the Association of Otolaryngologists of India* **70:** 425-427
54. Pootanakit K, Prior KJ, Hunter DD*, et al.* (1999) *Vis Neurosci* **16:** 221-230
55. Enz R (2012) *Front Mol Neurosci* **5:** 52
56. Enz R (2007) *Bioessays* **29:** 60-73
57. Rose M, Dütting E, Enz R (2008) *Journal of neurochemistry* **105:** 2375-2387
58. Mburu P, Kikkawa Y, Townsend S*, et al.* (2006) *Proc Natl Acad Sci U S A* **103:** 10973-10978
59. Okumura K, Mochizuki E, Yokohama M*, et al.* (2010) *Brain Res* **1307:** 53-62
60. Jean P, Ozcete OD, Tarchini B*, et al.* (2019) *Proc Natl Acad Sci U S A*, 10.1073/pnas.1818358116
61. Corti C, Battaglia G, Molinaro G*, et al.* (2007) *J Neurosci* **27:** 8297-8308
62. Linden AM, Johnson BG, Trokovic N*, et al.* (2009) *Neuropharmacology* **57:** 172-182
63. Pekhletski R, Gerlai R, Overstreet LS*, et al.* (1996) *J Neurosci* **16:** 6364-6373
64. Duvoisin RM, Zhang C, Pfankuch TF*, et al.* (2005) *The European journal of neuroscience* **22:** 425-436
65. Nouvian R, Eybalin M, Puel JL (2015) *Cell Tissue Res* **361:** 301-309
66. Ruel J, Wang J, Rebillard G*, et al.* (2007) *Hearing research* **227:** 19-27
67. Liberman MC (2016) *Advances in experimental medicine and biology* **875:** 1-7
68. Pujol R, Puel JL (1999) *Ann N Y Acad Sci* **884:** 249-254
69. Terreros G, Delano PH (2015) *Frontiers in systems neuroscience* **9:** 134
70. Masilamoni GJ, Smith Y (2018) *Curr Opin Pharmacol* **38:** 72-80
71. Valenzuela JC, Heise C, Franken G*, et al.* (2014) *Philosophical transactions of the Royal Society of London. Series B, Biological sciences* **369:** 20130606

FIGURE LEGENDS

Figure 1: Expression of group II and III mGluR types in the mouse cochlea. (**top**) Agarose gel showing PCR amplificates of expected size for the indicated mGluR types obtained from reverse transcribed transcripts purified from mouse cochlea. Expression of prominent C-terminal splice-variants of mGluR7 and mGluR8, termed a and b was analysed individually. The identity of PCR products was verified by sequencing. (**bottom**) Negative controls (H_2O) show primer-dimer formations (arrowhead), but no amplificates of the expected sizes. The left lane shows a 100 bp marker. For better visualization, black and white levels of the original photograph were inversed.

Figure 2: Localization of mGluR2/3 in cochlear wholemounts of gerbil and mouse. (A) Micrograph showing a cochlear wholemount from gerbil that was incubated with antibodies recognizing CtBP2/RIBEYE (red) to label the ribbon in pre-synaptic hair cell terminals and with DAPI (cyan) to visualize cellular nuclei. Co-staining with an immune serum recognizing a conserved epitope in mGluR2 and mGluR3 (mGluR2/3 - green) resulted in a punctate staining pattern in close vicinity to pre-synaptic ribbons. This is best seen in the magnification of the boxed region shown in the lower panel (**B**). The intensity of green and red fluorescent signals was measured along the white transparent arrows and compared in b´ and b´´. (**C, D**) Cochlear wholemounts from mouse were stained and analysed as described above.

Figure 3: Staining for mGluR2/3 overlaps with post-synaptic, but not with pre-synaptic markers. (A) Sketch of an IHC ribbon synapse depicting the distribution of used marker proteins relative to the synaptic cleft: CtBP2/RIBEYE labels the pre-synaptic ribbon (red) that is surrounded by glutamatergic vesicles (white circles), while PSD95 (magenta) serves as a post-synaptic marker. **(B)** Micrograph of a cochlear wholemount from mouse incubated with antibodies recognizing mGluR2/3 (green) and CtBP2/RIBEYE (red) and DAPI to mark cellular nuclei, as analysed by dual-colour STED microscopy. **(C)** The geometry of fluorescent signals was 3D reconstructed, centres of gravity for green and red labels were calculated (white balls) and their distances were measured (dashed line - a). **(F)** Similar analysis as in **(C)**, using the post-synaptic marker PSD95 (magenta) to measure distances, as indicated (black balls - b). **(D, E, G, H)** More examples of reconstructed signals. **(I)** Bar diagram comparing measured distances between mGluR2/3 and CtBP2/RIBEYE (a; n=8), or between mGluR2/3 and PSD95 (b; n=6). The number of synapses analysed is indicated in white. Three asterisks indicate a p-value < 0.0005.

Figure 4: Signals for mGluR2/3 are located at the IHC post-synapse, adjacent to the active zone. (A) Sketch of an IHC ribbon synapse showing the locations of pre-synaptic (CtBP2/RIBEYE - red, Bassoon – dark red) and post-synaptic (PSD95 - magenta) marker proteins relative to the synaptic cleft. **(B)** Overview of a 3D stack of confocal images from a cochlear wholemount of mouse that was incubated with antibodies recognizing the proteins indicated, or DAPI to mark cellular nuclei. The CtBP2/RIBEYE immune serum cross-reacts with IHC nuclei (asterisks). The background shows the same region in phase contrast (grey). **(C)** Reconstruction of the 3D geometry of fluorescent signals, as indicated. To visualize the distance between different labels more clearly, individual colour combinations are shown separately in the small panels to the right. **(D)** represents the same synapse as in **(C)**, rotated horizontally by approximately 90 degrees. For each colour, the centre of gravity (white dots) was calculated, and distances and angles were measured, as indicated. **(E)** More reconstructed synapses, labelled as indicated in **(C)**. **(F)** Bar diagrams summarizing calculated mean distances and angles between the centres of gravity of 42 synapses as shown in **(D).** White numbers represent the synapse quantity analysed. **(G, H)** Reconstruction and measurements of 13 3D reconstructed synapses as in **(D, F)** using Bassoon as pre-synaptic marker. p-values < 0.005 or 0.0005 are indicated by 2 or 3 asterisks.

Figure 5: The relation between mGluR2/3 clusters and IHC ribbons remains constant along the tonotopic axis. Cochlear wholemounts from mouse were incubated with antibodies recognizing mGluR2/3 (green) and CtBP2/RIBEYE (red). Images were taken from 3 regions indicated by the dashed boxes in the cochlear sketch shown in the middle, representing high (**A:** apex) middle (**B:** median) or low (**C:** base) frequencies. The number of green clusters (representing mGluR2/3) was counted and normalized to the number of red clusters, representing IHC ribbons. **(D)** Bar diagram comparing the number of mGluR2/3 positive clusters with the number of stained IHC ribbons. No statistical significant differences were observed. The number of analysed pictures for each cochlear region is given in white.

Figure 6: Synapsin 1 positive efferent terminals do not express mGluR2/3. Micrographs of cochlear wholemounts from mouse incubated with the immune sera indicated. Olivocochlear efferent terminals were marked with antibodies recognizing synapsin1. **(A)** While signals representing mGluR2/3 (green) and the pre-synaptic marker CtBP2/RIBEYE (red) are in close vicinity, label for Synapsin 1 (cyan) was observed at different locations. **(B)** To compare the distribution of fluorescent signals, the boxed region was enlarged, intensity profiles were measured along the white transparent arrow and are shown in the lower panel

(b´). **(C)** Micrographs analysed as in **(A)**, using the post-synaptic marker PSD95 (magenta) instead of CtBP2/RIBEYE. **(D)** As before, signal locations are compared along the transparent arrow and visualized in the lower panel (d´).

Figure 7: MGluR2, but not mGluR3 is located at the IHC post-synapse. Cochlear wholemounts were incubated with antibodies binding CtBP2/RIBEYE (red) to mark pre-synaptic ribbons of IHC, and with immune sera recognizing mGluR2/3 **(A)**, mGluR2 **(C)** or mGluR3 **(E)** (all in green). Fluorescent signals representing mGluR2/3 and mGluR2 were always located at the IHC ribbon synapse. This can be best seen in the enlargements of the boxed regions shown in **(B)** and **(D). I**ntensities of fluorescent signals were measured along the transparent arrows and compared in the lower panels (b´, d´). In contrast to mGluR2, the mGluR3 immune sera showed a more diffuse staining of low intensity within the region of IHC ribbon synapses. To ensure that these antibodies would recognize the native epitope of mGluR3, we co-stained primary cortical neurons for mGluR3 (green) and the synaptic marker protein Shank 2 (red) **(F).** Signal intensities were measured along the white arrow and resulting profiles are compared in f´.

Figure 8: MGluR4 is located at the pre-synaptic side of IHC ribbon synapses. (A) A cochlear wholemount of mouse was incubated with antibodies labelling pre-synaptic CtBP2/RIBEYE (red) and post-synaptic PSD95 (magenta) marker proteins and co-stained with an immune sera recognizing mGluR4 (green). The enlargements of the boxed region show a perfect superimposure of signals representing mGluR4 and CtBP2/RIBEYE **(B)**, while fluorescent label for mGluR4 and PSD95 were displaced **(C)**. This can be best seen in the comparisons of the signal intensities measured along the transparent white arrows (b´ + c´, b´´ + c´´). **(D)** The 3D geometry of fluorescent signals was reconstructed and shown, as described in Fig. 4C. **(E)** More reconstructed synapses, labelled as in **(D)**. At individual synapses the centres of gravity were calculated for each fluorescent label (black and white dots) and distances and angles were measured, as indicated. **(F, G)** Calculated mean distances and angles between the centres of gravity of 19 3D reconstructed synapses are summarized in the bar diagrams**.** White numbers represent the synapse number analysed. Three asterisks indicate a p-value < 0.0005.

Figure 9: IHC ribbon synapses express mGluR8b, but not mGluR8a. Cochlear wholemounts of mouse were incubated with immune sera recognizing mGluR8a **(A)** or mGluR8b **(B)**, together with antibodies binding to pre- or post-synaptic marker proteins, as indicated. While mGluR8a (green) was not co-localized with the pre-synaptic ribbon marker

CtBP2/RIBEYE (red), mGluR8b showed a perfect overlap with IHC ribbon synapses. This can be best seen in the two enlargements of the boxed region that compare the localization of mGluR8b (green) with the pre-synaptic marker protein CtBP2/RIBEYE (red) **(C),** or with the post-synaptic marker PSD95 (magenta) **(D)**. Comparing signal intensities for all 3 colours as measured along the white transparent arrows shows co-localization of mGluR8b with CtBP2/RIBEYE, while signals representing PSD95 are displaced (c´ + d´, c´´ + d´´). **(E - H)** The 3D geometry of fluorescent signals of 19 synapses was reconstructed, their centres of gravity were calculated, distances and angles were measured and graphically compared in bar diagrams, as explained in the legend of Fig. 8. Three asterisks indicate a p-value < 0.0005.

Table 1: Oligonucleotides used for expression analysis.

Overview of DNA sequences of used oligonucleotides. Primers amplify a C-terminal region of the receptor sequences and span an intron to detect potential amplification of chromosomal DNA. (P1 – sense primer; P2 – antisense primer, stop codons in the antisense primers are underlined).

Gene	Oligonucleotide [5´→ 3´]
mGluR2	P1 - CAGTGATTATCGGGTGCAG
	P2 - TCAAAGCGACGATGTTGTTGAG
mGluR3	P1 - TACACCACCTGCATCATCTG
	P2 - TCACAGAGATGAGGTGGTGG
mGluR4	P1 - CGGCTGACAAGCTGTACATC
	P2 - CTAGATTGCATGGTTGGTGTAAG
mGluR6	P1 - GTATTATCTGGCTGGCTTTCG
	P2 - CTACTTGGCGTCCTCTGAGTTC
mGluR7a/b	P1 - CACCCTGAACTCAATGTCCAG
mGluR7a	P2 - TTAGATAACCAGGTTATTATAACTG
mGluR7b	P2 - CTATACTGTTGGTGGGATAGTG
mGluR8a/b	P1 - CACGTGCATCATTTGGTTAGC
mGluR8a	P2 - TCAGATTGAATGATTACTGTAGC
mGluR8b	P2 - TTAGGAAGTGCTCCCGCTC

Table 2: Primary antibodies used in this study

Overview of primary antibodies used in this study. The epitope is characterized by species and amino acid region, if known. (aa – amino acids; NT seq. - N-terminal sequence)

Protein	Epitope	Dilution	Serum type	Reference
Bassoon	rat Bassoon	1: 400	mouse monoclonal	Enzo Life Sciences (ADI-VAM-PS003)
CtBP2/RIBEYE	mouse aa 361-445	1: 300	mouse monoclonal	BD Bioscience (612044)
CtBP2/RIBEYE	rat aa 974-988	1:5000	guinea-pig polyclonal	Synaptic Systems (193003)
CtBP2/RIBEYE	rat aa 95-207	1:5000	guinea-pig polyclonal	Synaptic Systems (192104)
mGluR2/3	rat mGluR2 aa 860-872	1: 100	rabbit polyclonal	Merck Millipore (AB1553)
mGluR2	NT seq. of 47 aa	1: 150	mouse monoclonal	Abcam (AB15672)
mGluR3	NT seq. of 16 aa	1: 150	rabbit polyclonal	Abcam (AB188750)
mGluR4	rat aa 834-912	1: 150	rabbit polyclonal	[17]
mGluR8	human aa 34-514	1: 50	mouse monoclonal	R&D Systems (MAB5277)
mGluR8a	rat aa 886-908	1:1000	guinea-pig polyclonal	Chemicon (AB5362)
mGluR8b	mouse aa 886-908	1: 150	rabbit polyclonal	[18]
PSD95	mouse aa 64-247	1: 250	mouse monoclonal	Synaptic Systems (124011)
PSD95	mouse aa 1-100	1: 100	goat polyclonal	Abcam (AB12093)
Shank 2	rat aa 1042-1475	1:1000	rabbit polyclonal	Synaptic Systems (162202)
Shank 2	rat aa 1042-1475	1:5000	guinea-pig polyclonal	Synaptic Systems (162204)
Synapsin 1	mouse aa 445-462	1:1000	guinea-pig polyclonal	Synaptic Systems (106104)

Figure S1: Verification of antibody specificity in primary cultures of cortical cells. Immune sera for mGluR2/3, mGluR2, mGluR3, mGluR4, mGluR8a, or mGluR8b were co-incubated with antibodies recognizing the post-synaptic marker protein Shank 2, as indicated. All receptor antibodies generated green fluorescent puncta that were located at or close to Shank 2-positive structures (red). This can be better seen in the enlargements of the boxed regions that are shown in individual colours. Obvious co-localizations of fluorescent signals are indicated by arrowheads. DAPI visualizes cellular nuclei.

Figure S2: Verification of the specificity of mGluR2 and mGluR3 immune sera in HEK-293 cells. HEK-293 cells were transfected with plasmids encoding for mGluR2 (upper 3 panels) or mGluR3 (lower 3 panels). Incubation with the mGluR2 immune sera stained cells expressing mGluR2 **(A)**, but not cells expressing mGluR3 **(B)**. In contrast, the mGluR3 immune sera did not recognize cells expressing mGluR2 **(C)**, but stained cells expressing mGluR3 **(D)**. The mGluR2/3 serum served as positive control for plasmid transfection and protein expression **(E, F)**. DAPI was used to visualize cellular nuclei.

Figure S3: Verification of the specificity of mGluR8a and mGluR8b immune sera in HEK-293 cells. Plasmids encoding for mGluR8a (upper 3 panels) or mGluR8b (lower 3 panels) were transfected in HEK-293 cells. The mGluR8a specific antibodies stained only cells expressing mGluR8a **(A)**, but not mGluR8b **(B)**. In contrast, the mGluR8b serum did not recognize cells expressing mGluR8a **(C)**, but mGluR8b **(D)**. Antibodies recognizing both mGluR8 variants served as positive control for plasmid transfection and protein expression **(E, F)**. DAPI was used to visualize cellular nuclei.

Figure 1

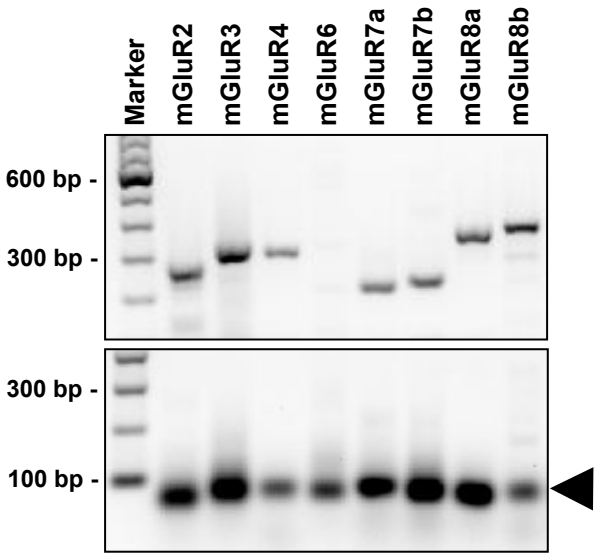
Marker
mGluR2
mGluR3
mGluR4
mGluR6
mGluR7a
mGluR7b
mGluR8a
mGluR8b
600 bp -
300 bp -
300 bp -
100 bp -

Figure 2

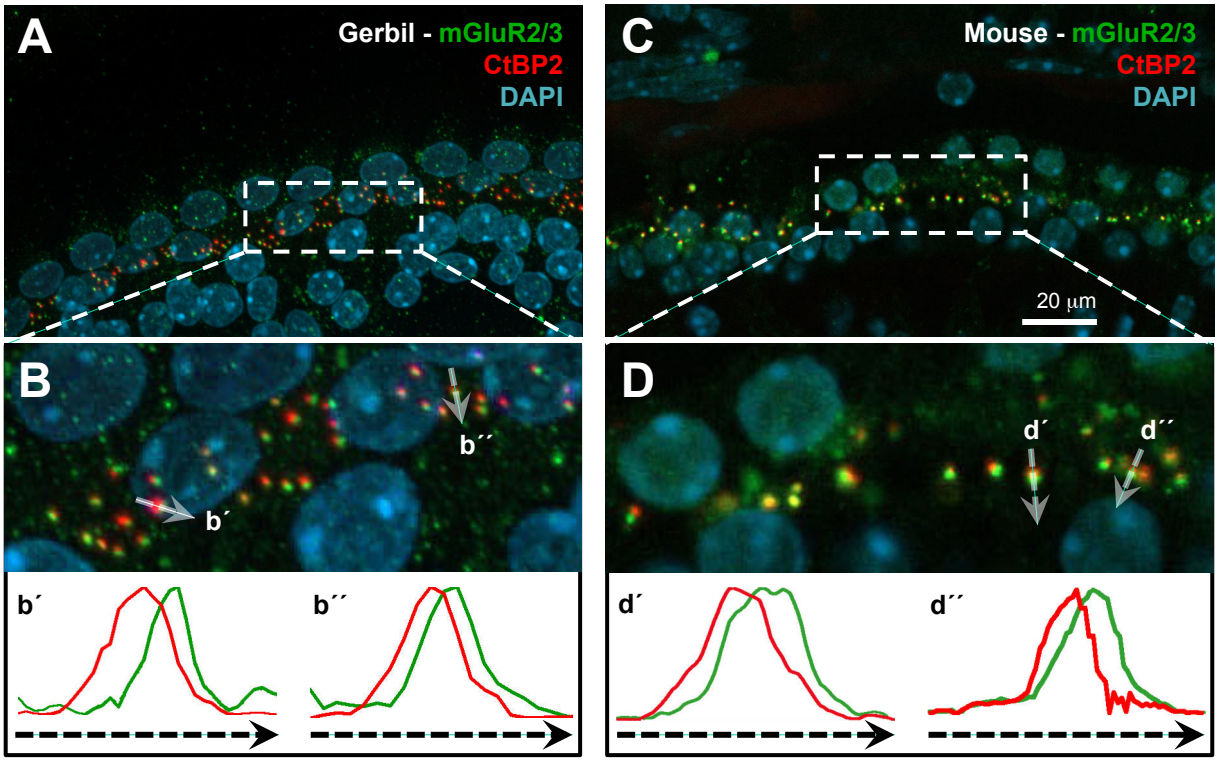
A
Gerbil - mGluR2/3
CtBP2
DAPI
B
b´
b´´
b´
b´´
C
Mouse - mGluR2/3
CtBP2
DAPI
20 µm
D
d´
d´´
d´
d´´

Figure 3

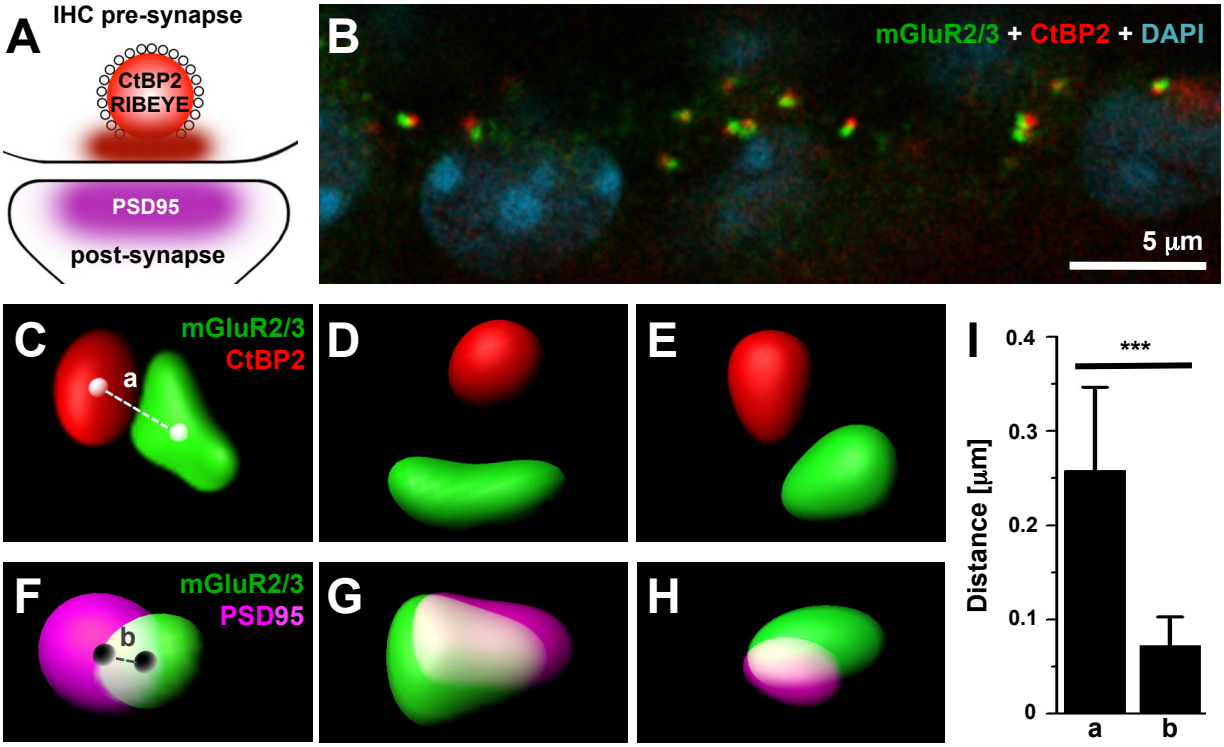
A
IHC pre-synapse
CtBP2
RIBEYE
PSD95
post-synapse
B
mGluR2/3 + CtBP2 + DAPI
5 µm
C
mGluR2/3
CtBP2
a
D
E
F
mGluR2/3
PSD95
b
G
H
I
Distance [µm]
0.4
0.3
0.2
0.1
0
***
a
b

Figure 4

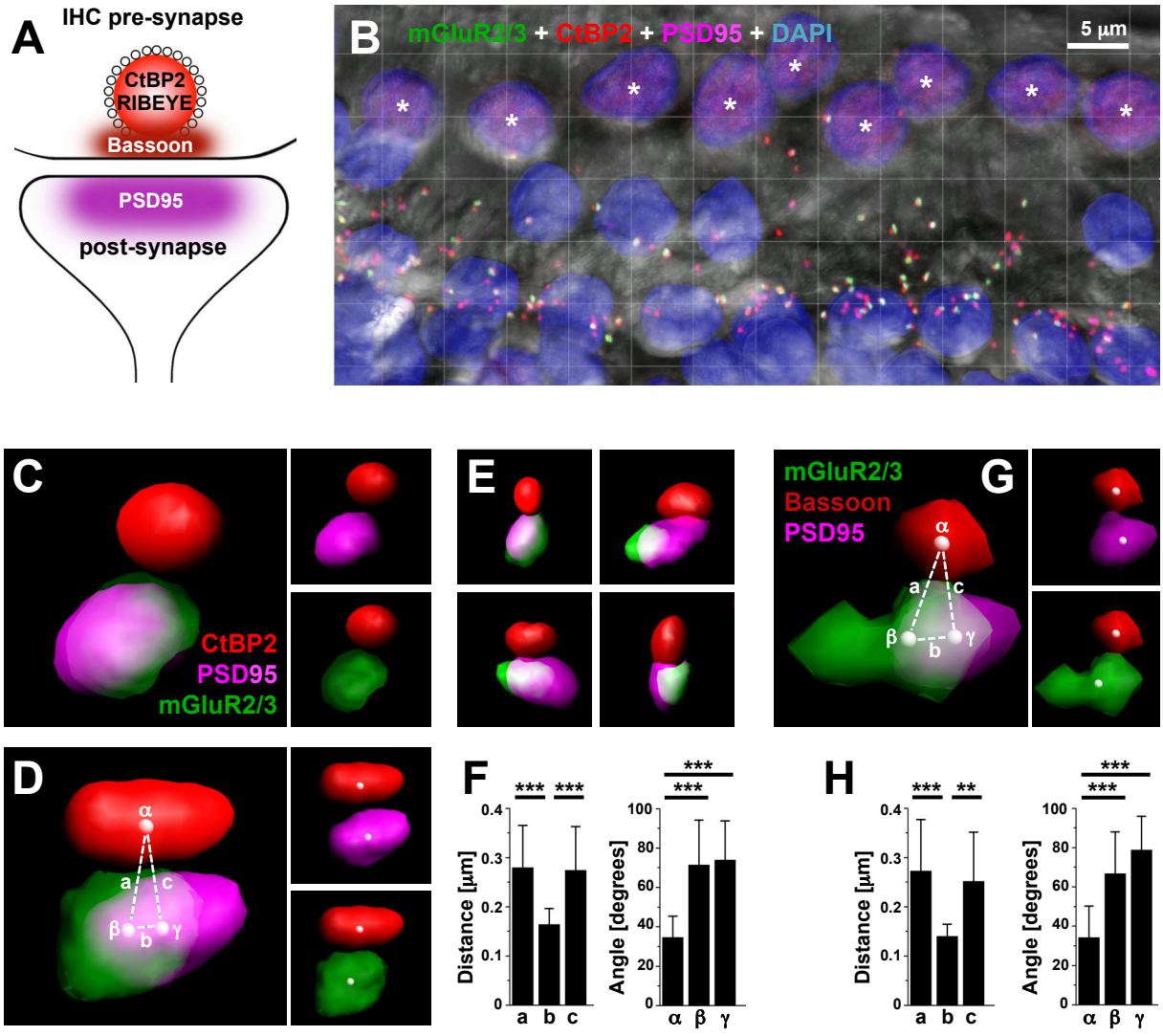
A
IHC pre-synapse
CtBP2
RIBEYE
Bassoon
PSD95
post-synapse
B
mGluR2/3 + CtBP2 + PSD95 + DAPI
5 µm
C
CtBP2
PSD95
mGluR2/3
D
α
a
c
β
b
γ
E
mGluR2/3
Bassoon
PSD95
G
F
***
***
***
***
Distance [µm]
0.4
0.3
0.2
0.1
0
a b c
Angle [degrees]
100
80
60
40
20
0
α β γ
H
***
**
***
***
Distance [µm]
Angle [degrees]

Figure 5

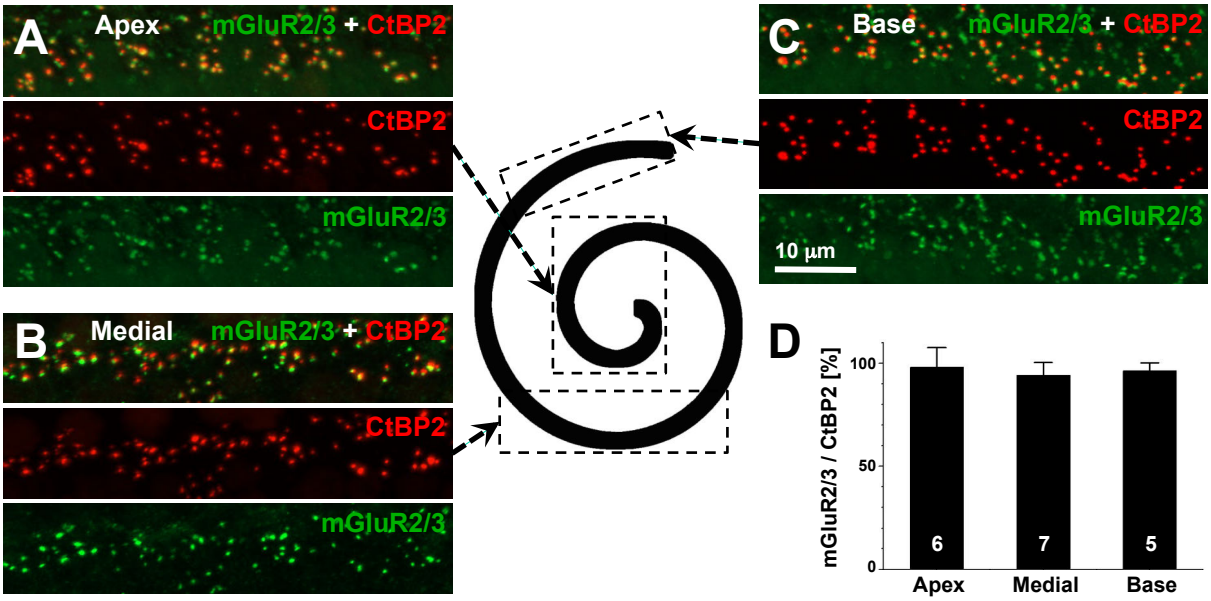
A
Apex
mGluR2/3 + CtBP2
CtBP2
mGluR2/3
B
Medial
mGluR2/3 + CtBP2
CtBP2
mGluR2/3
C
Base
mGluR2/3 + CtBP2
CtBP2
mGluR2/3
10 µm
D
mGluR2/3 / CtBP2 [%]
100
50
0
6
7
5
Apex
Medial
Base

Figure 6

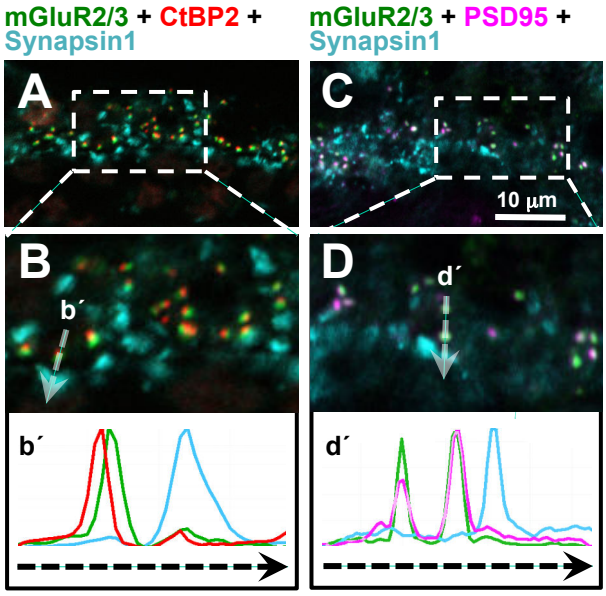
mGluR2/3 + CtBP2 +
Synapsin1
mGluR2/3 + PSD95 +
Synapsin1
A
B
b´
b´
C
10 µm
D
d´
d´

Figure 7

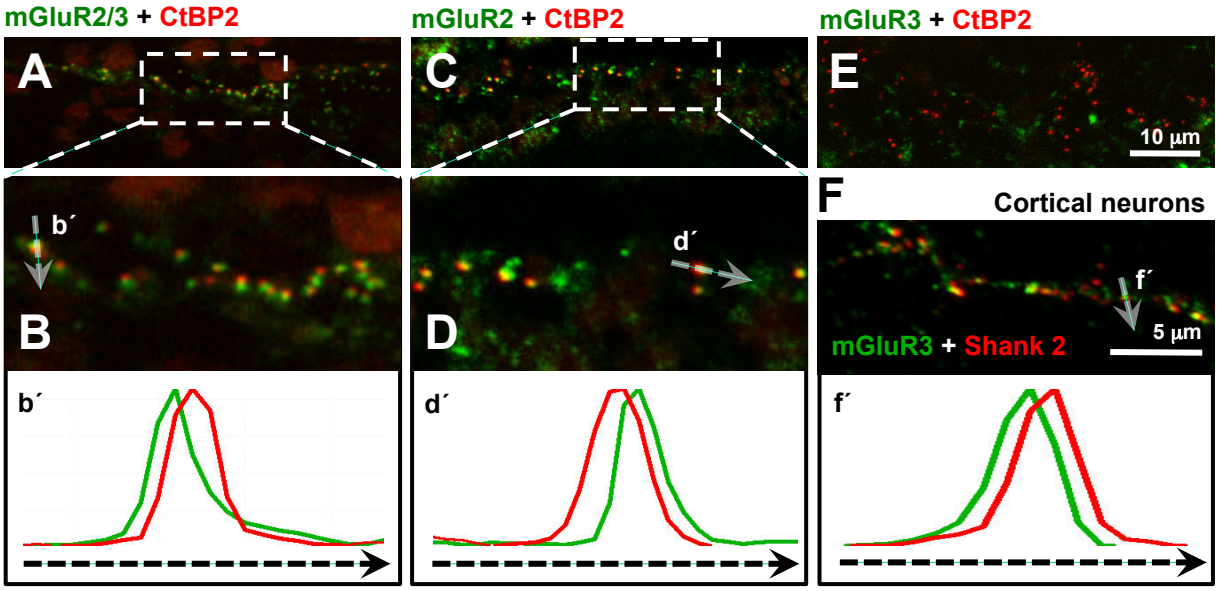
mGluR2/3 + CtBP2
mGluR2 + CtBP2
mGluR3 + CtBP2
A
C
E
10 µm
b´
d´
B
D
F
Cortical neurons
f´
5 µm
mGluR3 + Shank 2
b´
d´
f´

Figure 8

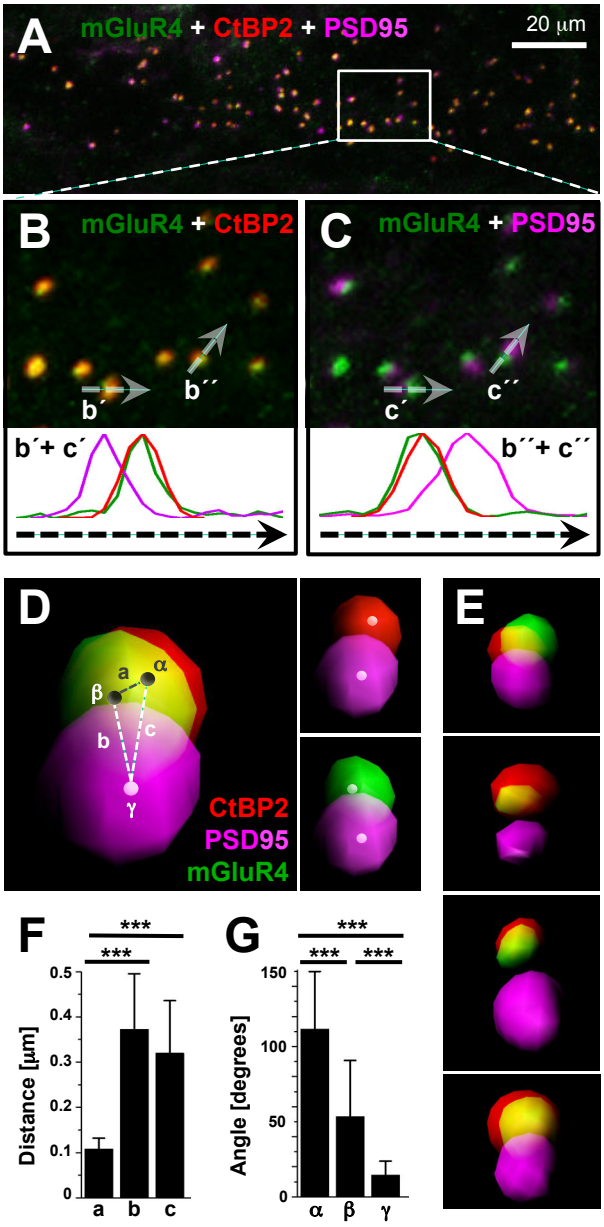
A
mGluR4 + CtBP2 + PSD95
20 µm
B
mGluR4 + CtBP2
b´
b´´
b´+ c´
C
mGluR4 + PSD95
c´
c´´
b´´+ c´´
D
a
α
β
b
c
γ
CtBP2
PSD95
mGluR4
E
F
***
***
Distance [µm]
0.5
0.4
0.3
0.2
0.1
0
a b c
G
***
***
***
Angle [degrees]
150
100
50
0
α β γ

Figure 9

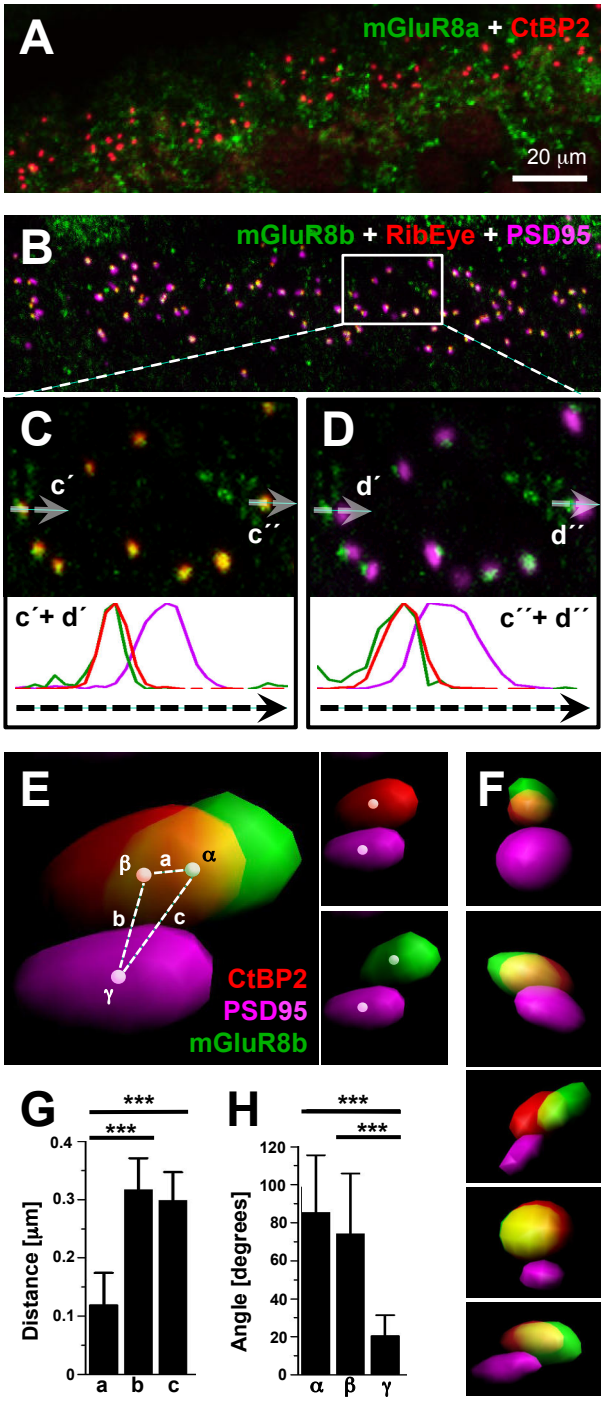
A
mGluR8a + CtBP2
20 µm
B
mGluR8b + RibEye + PSD95
C
c´
c´´
c´+ d´
D
d´
d´´
c´´+ d´´
E
α
β
γ
a
b
c
CtBP2
PSD95
mGluR8b
F
G
***
***
Distance [µm]
0.4
0.3
0.2
0.1
0
a b c
H
***
***
Angle [degrees]
120
100
80
60
40
20
0
α β γ

Supplementary Figure 1

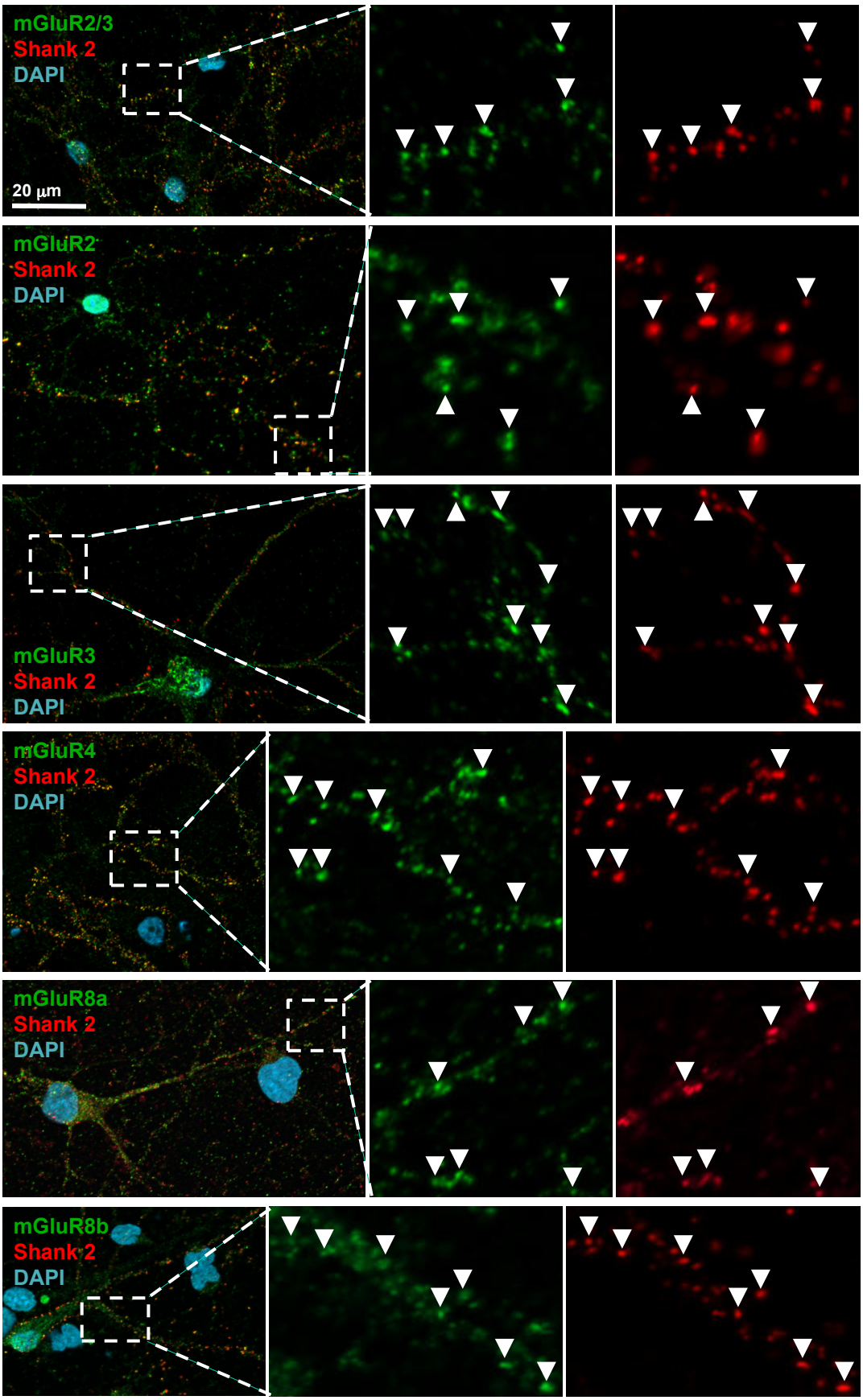

Supplementary Figure 2

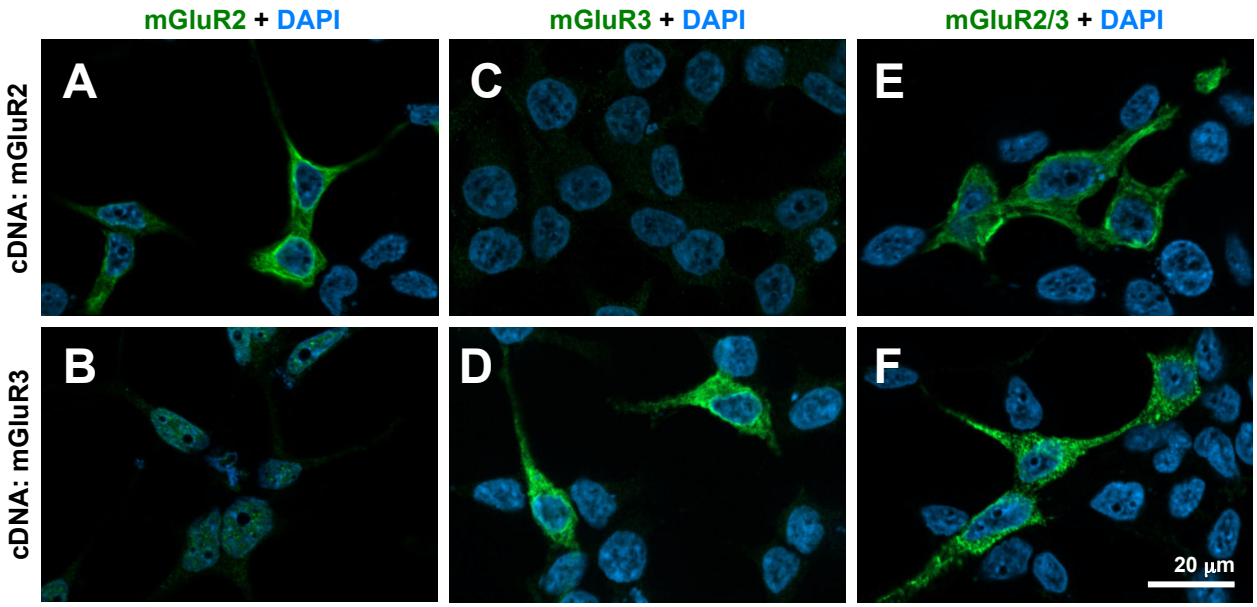

Supplementary Figure 3